

Lessons Learned from the Launch of a Student-Built Jet-A/Liquid Oxygen Rocket

Rithvik Nagarajan¹, Ethan Heyns², Braden Anderson³, Michael Krause⁴,
Callum MacDonald⁵, Varun Natarajan⁶, Anthony Otlowski⁷, and Tristan Terry⁸
Georgia Institute of Technology, Atlanta, GA 30332

The Yellow Jacket Space Program (YJSP) is a student organization at Georgia Tech working to develop liquid propellant rockets with the goal of launching a vehicle beyond the Kármán Line to the edge of space. From August 2020 to January 2023, students designed, built, and launched a subsonic test vehicle named GoldiLOX. This liquid oxygen and Jet-A pressure-fed rocket achieved a measured thrust of 1000 lbf and reached a 5000 ft apogee, marking a significant milestone as the first successful liquid rocket launch and recovery by Georgia Tech. Vehicle propulsion and flight data was retrieved successfully, and the following paper presents an in-depth analysis of the vehicle's performance and highlights the lessons learned from launching a cryogenic liquid sounding rocket.

I. Nomenclature

A	=	area
A_t	=	nozzle throat diameter
C_dA	=	coefficient of discharge multiplied by area
c^*	=	characteristic velocity
DOF	=	degree of freedom
GN_2	=	gaseous nitrogen
IMU	=	inertial measurement unit
IT	=	vehicle intertank
LOX	=	liquid oxygen
\dot{m}	=	mass flowrate
MR	=	propellant mixture ratio; $\frac{\dot{m}_{oxidizer}}{\dot{m}_{fuel}}$
P	=	pressure
p_c	=	chamber pressure
ρ	=	density
$COPV$	=	composite overwrapped pressure vessel
$Jet-A$	=	commercial aviation-grade jet fuel
FOD	=	foreign object debris

¹ Co-Chief Engineer, Aerospace Engineering, AIAA Graduate Student Member.

² Co-Chief Engineer, Aerospace Engineering, AIAA Undergraduate Student Member.

³ Structures Lead, Mechanical Engineering, AIAA Undergraduate Student Member.

⁴ Flight Dynamics Lead, Aerospace Engineering, AIAA Graduate Student Member.

⁵ Propulsion Lead, Aerospace Engineering, AIAA Undergraduate Student Member.

⁶ Recovery Lead, Aerospace Engineering, AIAA Undergraduate Student Member.

⁷ Vehicle Fluids Co-Lead, Aerospace Engineering, AIAA Undergraduate Student Member.

⁸ Vehicle Fluids Co-Lead, Aerospace Engineering, AIAA Undergraduate Student Member.

II. Introduction

In 2015, students at the Georgia Institute of Technology founded the Yellow Jacket Space Program (YJSP), a rocketry club with the ambitious goal of developing, testing, and launching a liquid propelled hypersonic rocket to the edge of space. YJSP prepares students for the aerospace industry through challenging experiences gained from working with custom hardware including engines, valves, electronics, and structures. The organization offers a learning environment for students to apply classroom knowledge to practical projects. Over 8 years, the program grew to over 200 active students including undergraduate and graduate students from a variety of schools including Aerospace, Mechanical, and Electrical Engineering, as well as Computer Science and Business [1].

YJSP spent 3 years designing a Kerosene and Liquid Oxygen Heat-Sink Engine [2], Engine Test Stand, and associated hardware including custom valves and electronics. This effort culminated in 2019 with a Hot Fire test that achieved 700 lbf thrust and 210 psia chamber pressure. From then, students started designing a subscale vehicle named GoldiLOX, a proof-of-concept for a larger space-shot vehicle with the intent to prove YJSP's design methodology, testing strategy, and give expected performance characteristics for a bigger, more complex vehicle. This design effort resulted in a Preliminary Design Review (PDR) in January 2021 where students presented the vehicle design to aerospace faculty and industry members.

Throughout 2021 and 2022, students built and tested the vehicle numerous times with inert cold flows and fully integrated static fire tests. The first and second static fires, in November 2021 and April 2022 respectively, resulted in engine hard starts and no thrust data. After iterating on valve, injector, and igniter designs, the third static fire in November 2022 was successful, validating the flight feed system's ability to deliver propellants into the engine to produce the desired thrust for launch.

In January 2023, students traveled to the Mojave Desert to launch GoldiLOX. After 3 days of final vehicle integration and checkouts, GoldiLOX was successfully launched and recovered. With only minor damage sustained during impact due to a recovery system anomaly, students were able to retrieve all propulsion and flight data from the launch detailing the performance of all the vehicle systems. The following sections present an analysis of the retrieved data and highlight lessons learned from the launch.

III. Vehicle Design

Mission success criteria included launching the vehicle off the launch rail with high stability, achieving the expected MECO without anomaly, reaching the target apogee of 1000 m with dynamic stability, and achieving soft touchdown with an intact vehicle through a successful recovery system.

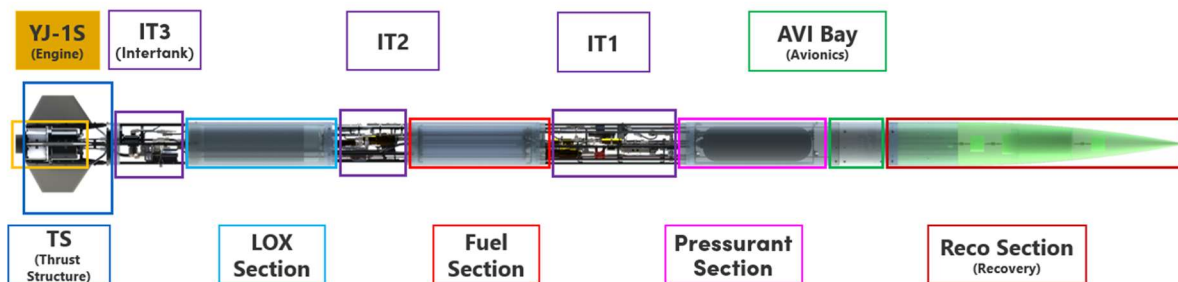


Fig. 1 GoldiLOX Layout.

Given those criteria, the vehicle was designed with five primary systems: the structure, engine, fluid feed system, avionics, and recovery system. These five vehicle systems, coupled with ground support equipment (GSE), were required for safe launch operations. The vehicle is 18 ft long and has an 8 in diameter airframe. Propellant and pressurant tanks are mounted within the airframe and are joined by intertank (IT) sections, which house the feed system components. The engine was mounted to the thrust structure and was designed to provide 785 lbf of thrust over an 8 second burn. The fluid feed system is pressure-fed using dome loaded regulators to control gaseous nitrogen

(GN2) pressure in each propellant tank. Through tank pressurization, 0.66 kg/s of Kerosene (Jet-A) and 1.19 kg/s of liquid oxygen (LOX) are delivered to the engine. The avionics system, located within the AVI bay, commands the valves and recovery triggers, collects propulsion and flight data, and communicates with mission control allowing fully remote operation of the vehicle. A complete list of sensors read by the avionics system are listed in Table 1. The recovery system uses barometer data to trigger a single-stage reefed parachute deployment and disreef to slow the vehicle descent for a soft landing of 7.62 m/s.

Table 1 GoldiLOX on-board sensors

	Part Number	Accuracy	Vehicle Locations
Pressure Transducer	Gems 3200	0.5% FS	COPV, LOX Tank, LOX Injector, Fuel Tank, Fuel Injector, Engine Chamber
Inertial Measurement Unit (IMU)	MTi-1	± 6 deg/h ± 40 μ g	Avionics Bay
Barometer	MS5611	± 1.5 mbar	Avionics Bay
GPS	Maestro A2200	< 2.5m CEP	Avionics Bay

IV. Trajectory Analysis

Three analyses of the flight trajectory are presented—vehicle stability, vertical flight profile, and landing position. In the latter two cases, direct comparisons are provided between the flight data and Monte Carlo (MC) simulations run immediately prior to launch, using live atmosphere data. Coincident with vehicle design, YJSP developed an in-house six degree-of-freedom (6DOF) trajectory simulator in MATLAB, with MC capabilities. Vehicle and environmental properties such as propellant mass, aerodynamic coefficients, and launch rail tilt were modeled probabilistically to establish performance envelopes. Live weather data was ingested from NOAA servers by the simulator for launch day support [3].

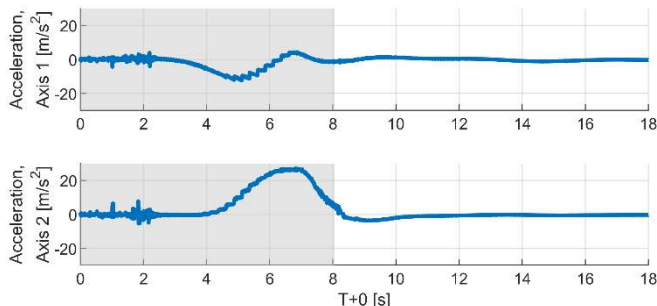


Fig. 2 Accelerometer measurements orthogonal to long axis. Powered flight shaded gray.

Stability characteristics are typically determined by examining the response of the vehicle to a perturbation in angle of attack [4]. Unfortunately, measuring angle of attack on a launch vehicle is a difficult task [5], and GoldiLOX had no way to obtain this data directly. Despite this, examining accelerometer data provides insight into relevant vehicle motion. Figure 2 shows readouts of the two accelerometer channels orthogonal to the long axis of the vehicle immediately after launch. While the clocking of this sensor relative to the inertial frame was not well-recorded (thus preventing quantitative comparison against simulated sensor data), important qualitative results may still be drawn. The vehicle moved along the rail during the first two

seconds of flight, which caused heavy vibrations that show up as noise in the sensors. This is examined in Section VIII. Immediately after departure from the rail, the vehicle was no longer constrained to be vertical and began to pick up horizontal components of acceleration. If the perturbation causing this horizontal acceleration was purely aerodynamic, the vehicle would have been expected to damp out this acceleration [4] – however, this lateral acceleration built roughly until engine shutdown. Off-axis engine mounting (and subsequent off-axis thrust) provides the best explanation for this phenomenon. Upon inspection of Figure 2, once engine shutdown ended around T+8 seconds and the vehicle motion became a function only of aerodynamic forces and gravity, the vehicle damped out its residual nonzero angle of attack as a slightly underdamped second order system, as expected.

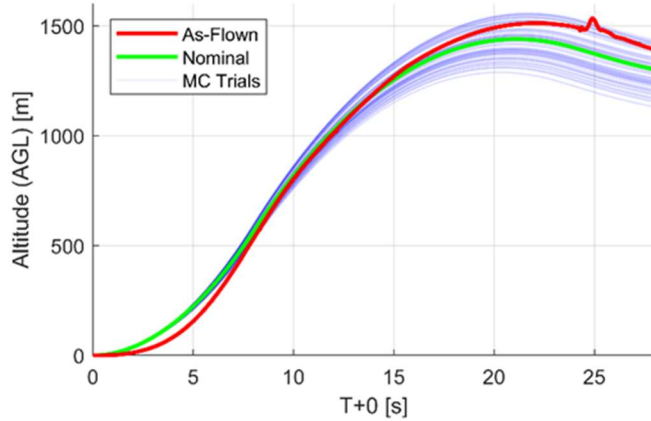


Fig. 3 Altitude profile overplotted against day-of-launch Monte Carlo simulations.

While the altitude estimation and performance show good agreement, the same cannot be said for the estimation of the landing site. This discrepancy appears to be a function of the same thrust misalignment observed in the stability analysis. While off-axis thrust was modeled in the various Monte Carlo trials, it was not perturbed to the extent that would have been necessary to produce such a dramatic departure from the expected trajectory direction. Most of the trajectory dispersions were dominated by winds—both on ascent, where winds perturb the local angle of attack, and on descent, where winds tend to carry the vehicle under parachute. During flight, the influence of the off-axis thrust was dramatically greater than that of the winds and caused a strong deviation from the expected landing ellipses. Figure 4 illustrates this difference with an overlaid plot between the expected landing ellipses and the actual landing location. The three-sigma ellipse predicts a maximum downrange distance of ~ 0.7 km, but the landing site was ~ 1.1 km from the launch location. This discrepancy highlights the need for more cross-team vehicle modeling efforts, as well as the clear incorporation of as-built configurations in simulations as the vehicle design and build matures.

Altitude data was obtained through sensor fusion with the IMU and GPS. Figure 3 shows the altitude of the vehicle over time during ascent, apogee, and the initial portion of descent. The thrust followed an unexpected curve – initially low, then increasing over flight – the cause of which is further examined in Section VII. As compared to Monte Carlo simulation, the flight initially fell below the expected envelope of trajectories, before “catching up” and falling within the upper bounds of the simulated trajectories. Ultimately, this delivered satisfactory confidence in the altitude estimation portion of the 6DOF, as well as confirming expected total impulse from the engine.

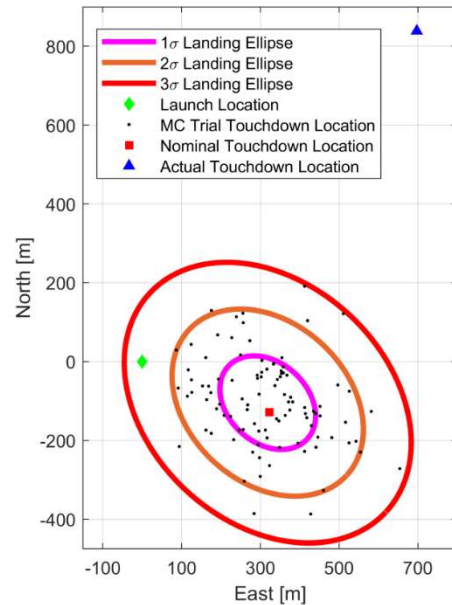


Fig. 4 Anticipated landing ellipses compared to actual landing site.

V. Recovery Analysis

The primary objective of the recovery (RECO) system was to prevent damage due to vehicle impact by achieving a safe landing velocity using a reefed parachute. Reefing is accomplished by running a line around the skirt of the parachute to initially constrict its drag-area; the reefing line is subsequently cut to fully inflate the parachute. The RECO system was mostly effective, as minimal damage was sustained to the vehicle upon impact, but there was notable damage to the parachute.



When the vehicle was recovered after launch, a large tear in the parachute along one of the seams

Fig. 5 Recovered parachute at landing site.

was observed. The riser and suspension lines were untangled and undamaged, indicating that the parachute was properly packed in the deployment bag. There was no visible damage to the nosecone, which was found detached from the vehicle. Further hardware inspection was conducted post launch.

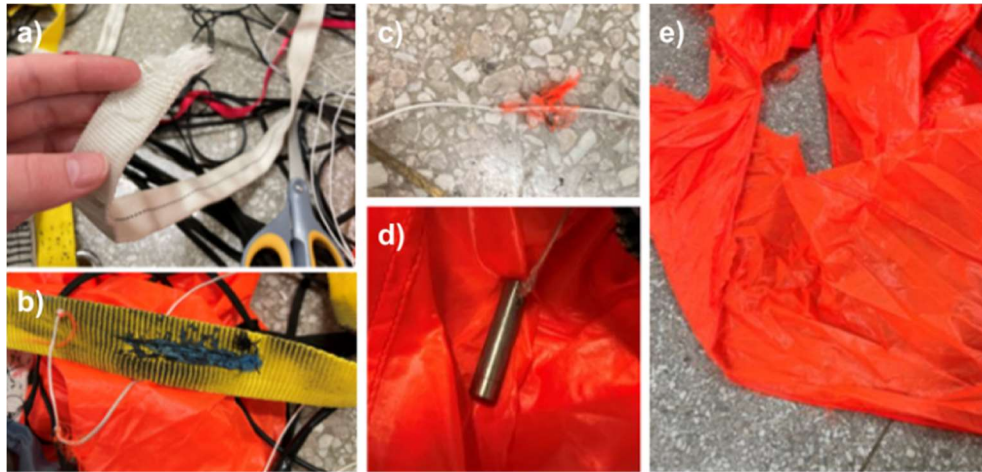


Fig. 6 a) Severed Nosecone Riser, b) Damaged Cable Loop, c) Slipped Knot, d) Actuated Line Cutter, e) Parachute Hole.

One of the double fisherman knots holding the reefing line was found to have slipped, indicating that the knot was not strong enough to withstand the initial opening force. The cables running from the RECO computer to the line cutters were also cleanly sheared near the skirt of the parachute. Based on this evidence, it was concluded that the asymmetric force caused by the knot slipping and tension from the cable lines caused the parachute to rupture after deployment. The recovery phases derived from flight data are indicated on Figure 7.

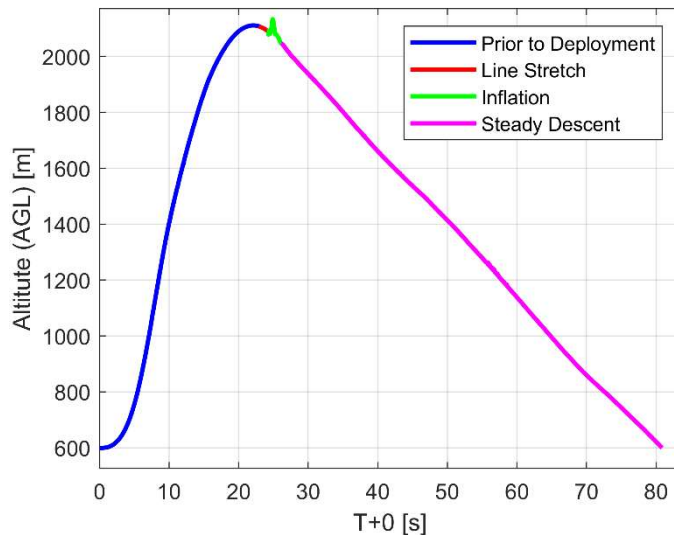


Fig. 7 RECO Phases Indicated on Altitude Plot.

Approximately 1 second after apogee, the nosecone deployment charge ignited. The vehicle reached a descent velocity of 24.6 m/s after initial inflation, and the vehicle continued to descend at this velocity until touchdown. Since the descent velocity of the vehicle remained relatively constant after T+30 seconds, earlier than the vehicle reached the disreef altitude of 304.8 m (1000 ft), parachute disreefing was likely unsuccessful. Additionally, the descent velocity was higher than the goal of 7.62 m/s. In terms of improvements to the RECO system, the transient deployment behavior should be considered in further detail in the development process. Seemingly minor design decisions, such as the choice of reefing line knot and cable, can be the difference between a successful and unsuccessful recovery operation.

VI. Engine Analysis

Thrust data was derived using acceleration data from the on-board IMU. The ideal thrust was calculated using the measured chamber pressure and engine geometries [6]. Excluding the startup transient behavior, there was a positive linear trend in the thrust supported in both the IMU Measured Thrust and Ideal Thrust plots. While a typical engine would see small increases in thrust as the vehicle ascends and ambient pressure decreases, the low maximum altitude and pressure plot rule out this as an option. Diving deeper into the pressure data, the fuel and oxidizer injector pressures also increase over the duration of the burn, though at different rates. The reasoning behind that behavior, related to the coupled physical response of the pressure regulators, will be discussed in Section VII.

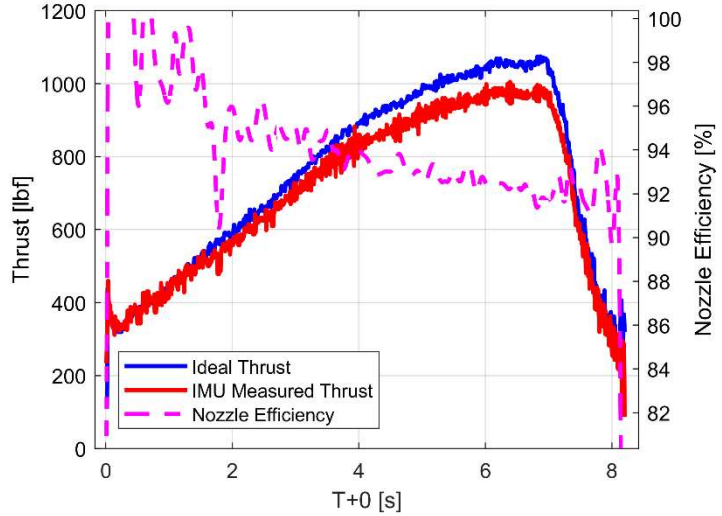


Fig. 8 GoldiLOX Measured Thrust and Nozzle Efficiency.

Figure 9 contains data pertaining to the combustion efficiency of the engine, which is the main source of inefficiency in the engine, as the combination of stagnation pressure loss and divergence of the flow is marginal in comparison. The “ideal” C^* efficiency was calculated using NASA’s CEA [7] program in which chemical equilibrium is assumed. The calculated C^* efficiency was determined using the measured chamber pressure, nozzle throat, and mass flow with Equation 1 [6].

$$c^* = \frac{p_c A_t}{\dot{m}} \quad (1)$$

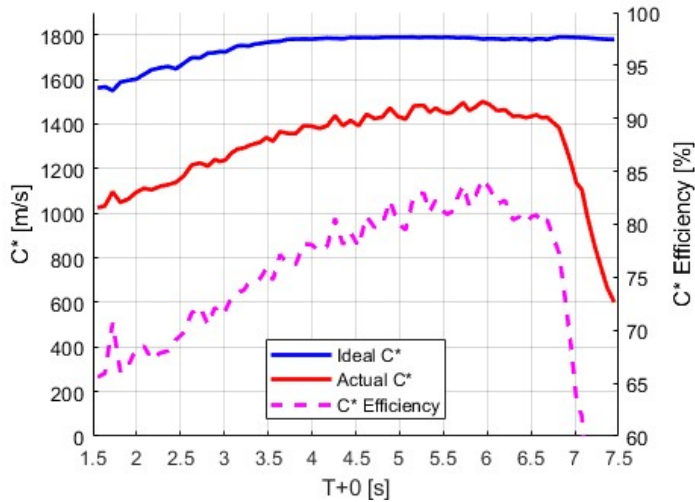


Fig. 9 Engine Combustion Performance.

Over the rest of the burn the performance did increase as the engine got closer to the proper operating condition but still yielded a low combustion efficiency of 80%. Since engine performance is so closely coupled to the feed system behavior in a pressure-fed vehicle, it is critical that future engine testing isolates performance of the engine. This could be achieved with more precising metering of propellant flowrates using dedicated sensors on an engine test stand.

The performance is poor at the beginning of the burn, likely due to the far off-nominal mixture ratio which created low thrust and threw off the mixing performance of the pintle injector. It is important to note that the pressure plot does not reveal the whole story. Visually, the engine startup was rich, with unburnt Jet-A casting a wide flame over the launch pad while the plume itself was dark and sooty, shown in Figure 10, and clearly apparent upon inspection of the chamber post flight in Figure 11. This brings scrutiny to the fuel pressure data, which may have been affected by debris plugging up the line to the pressure transducer. It is likely that the true fuel condition would be closer to the linear extrapolation of the pressure data on the left-hand side of Figure 9. This behavior would correlate with fuel tank pressure data and throw off mixture ratio that would yield a similar “ramping” performance as the oxygen pressure rose to its nominal value.

Extensive testing and improved data collection will drive the development of better injectors that result in higher engine efficiencies for the next generation of YJSP vehicles.



Fig. 10 GoldiLOX Engine Burn at T+0.76.



Fig. 11 Inspection of Injector Post Launch.

VII. Fluid Feed System Analysis

The primary objective of the vehicle feed system is to deliver the propellants to the engine at the designed pressures and mass flow rates. Specifically, the pressure differential across the injector from the feed system to the combustion chamber should be controlled such that stiffness requirements are met and the resulting mass flow through the injector restriction is correct. Several phenomena require characterization to enable injector pressure determination, including viscous pressure losses in lines, pressure losses in components, tank pressure regulator droop (defined as the decreasing of output pressure with increasing flow rate), and offsets between the set and output pressures of the dome-loaded tank regulators [6].

Table 2 Predicted and Observed Pressure Ladder and Properties

	Fuel Side		LOX Side	
	Expected Value	Launch Value	Expected Value	Launch Value
Regulator Offset	86 psid	87.7* psid	120 psid	116.2* psid
Droop	139 psid	131* psid	177 psid	306.8* psid
Liquid Pressure Loss	92 psid	106.6 psid	19 psid	45.6 psid
Beginning of Flow Tank Pressure	402.3 psia	412.5 psia	494 psia	210 psia
System C_dA	0.207 cm ²	-	0.319 cm ²	-
Propellant Mass Flowrate	0.663 kg/s	-	1.19 kg/s	-

The determination of propellant mass flow is central to predicting the performance of the vehicle propellant feed system. With the absence of traditional flow meters on the vehicle, Equation 2 was used in previous testing to derive a C_dA value for the entire feed system. This value, known as the system C_dA , allows the calculation of mass flow rate given a pressure difference between the tank pressure and engine main injector plate outlet for each commodity. The system C_dA values are used to determine the ideal steady-state tank pressures under nominal engine operating conditions. To achieve these steady-state tank pressures, the vehicle's regulators need to be set at a value higher than the desired tank pressure to account for various effects including regulator droop and an empirically derived offset

between the dome load pressure and the static outlet pressure. Regulator droop was modeled computationally through an iterative duo-variable-area orifice calculation utilizing coefficients anchored in test data. The offset between set regulator pressure to dome-loaded regulator output pressure was found to be statistically un-modellable and was only predicted through averaging tank pressurization data. Combining all the analytical and empirical models for the various effects on injector pressure, the expected pressure ladder for launch conditions was constructed, and the target set pressures and tank pressures were identified. Table 2 shows the expected pressure ladder compared to the actual observed launch conditions – noting that the asterisks indicate time averaged values over the burn.

$$C_d A = \frac{\dot{m}}{\sqrt{2\rho\Delta P}} \quad (2)$$

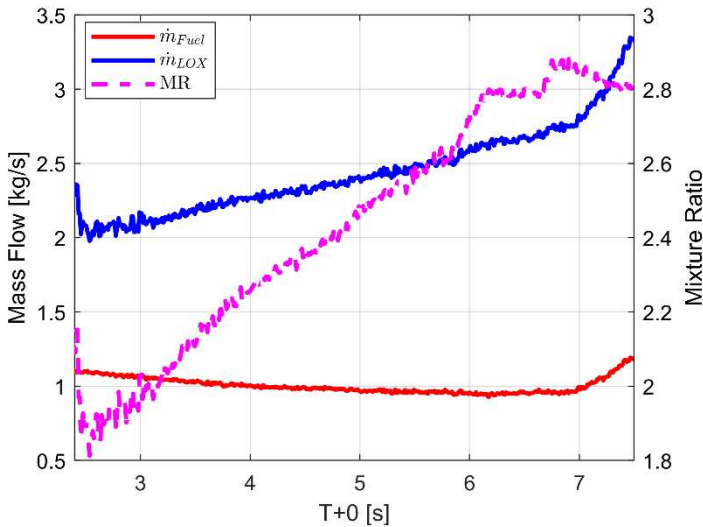


Fig. 12 Propellant Mass Flows and Mixture Ratio

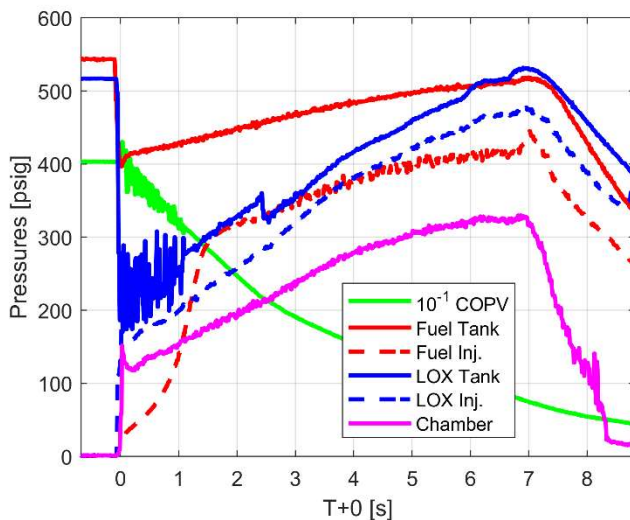


Fig. 13 Tank, Injector, and Engine Chamber Pressures

Disregarding the anomalous initial behavior of the fuel injector pressure transducer, which was likely caused by foreign object debris (FOD) clogging the fuel pressure transducer, fuel mass flow began higher than expected and moved closer to the nominal value at the end of the burn before spiking during the shutdown transient. The LOX mass flowrate initially fell to less than 1 kg/s due to high regulator droop, but it steadily increased throughout the entire burn. About halfway through the burn, both mass flows were approximately equal to their designed value, and LOX continued to rise resulting in a maximum MR of almost 2.9, much higher than the expected MR of 1.8.

As seen by comparing Figure 13 and Table 2, pressure drop models predicted fuel-side pressure loss to within 10 psi, the resolution of the sensor; however, on the LOX-side, the model seemed to break down, under predicting pressure drop by ~27 psi. This result is not entirely unexpected as consistent values for system $C_d A$ of the LOX-side were never determined during flow campaigns; however, LN2 models were successfully created, thus the differences can largely be attributed to testing that did not properly replicate flight conditions.

The drastically higher droop observed in Figure 13 on the LOX-side, 130 psi higher than expected, is the root cause of most performance differences between models, static fires, and the actual flight. Curiously, however, both the fuel-side and LOX-side regulators are the exact same component purchased from the same vendor, and the computational droop model was largely successful in predicting droop on the fuel-side. The much higher observed droop value on the LOX regulator can be attributed to many different factors. One might be some event that triggered a much larger gas flowrate into the

tank on engine startup, such as a tank fluid height that covered the tank pressurization inlet. Another possible source for this behavior is a decreased intertank temperature causing the regulator seals to have increased friction, thus

increasing the response time for the regulator to keep up with the needed gas flowrate. A third explanation may be high leakage out of LOX fluid components increasing the LOX tank gas consumption and thus increasing droop. It is most likely that some combination of these explanations can fully explain the LOX-side regulator droop behavior.

Another significant observation is that both tank pressure sensors (and likewise all sensors downstream of the tanks) showed a significant pressure rise throughout the burn. Per manufacturer spec, the expected rise in the dome-loaded regulator's outlet due to the ~3200 psia change in COPV pressure would be approximately 32 psia; however, the fuel tank rose 96 psia and the LOX tank rose 305 psia. In previous static fire testing, the feed system did not show such drastic increases after the initial expected droop, so it seems as though differences between the flight environment and ground testing must be responsible. It is possible the acceleration directly affected the poppets within the dome-loaded regulators, causing them to open more as the acceleration increased throughout flight. Additionally, changing thermal collapse of GN2 in the LOX tank may have had a significant impact on the rising pressure in the LOX tank. Collapse would start out very high with a very cold LOX tank and high liquid volume and decrease as both the GN2 temperature decreases during its adiabatic expansion and the tank wall temperature increases. A lower collapse would mean a lower GN2 drawdown into the tank and thus lower droop, a theory somewhat consistent with the decreasing COPV outflow. The same cannot be said for the fuel-side pressurization behavior, but thermal effects present on both regulators, such as Joule-Thomson cooling [8] and adiabatic expansion of the GN2 may have also had effects previously undiscovered during ground testing. Unfortunately, the flight vehicle lacked instrumentation that would help confirm these explanations, such as ullage temperature sensors and COPV temperature sensors.

The anomalous feed system behaviors point to a major design decision that should be reconsidered on future vehicles: the implementation of active tank pressure control (TPC) [9]. Active TPC decouples the tank pressure from injector pressure, eliminates the need for long regulator characterization campaigns, allows for precise control of MR, and removes any acceleration effects that may have affected the regulators on GoldiLOX. Most issues during flight with the GoldiLOX feed system can be traced back to the uncharacterized behavior by the LOX side regulator, a problem eliminated if active TPC was used.

Overall, the vehicle feed system succeeded in its role as the primary goals of the mission were met and even exceeded; however, many key anomalies within the system point to the idea that the GoldiLOX feed system is a flawed design under flight conditions, a conclusion that was not and could not be determined from the data captured during ground testing. Better steps should be taken to match flight conditions on the ground, including doing full duration static fires, but some effects, such as those from acceleration and in-flight dynamics, have no substitute without flight data.

VIII. Vehicle Structure Analysis

The vehicle structure performed nominally through flight with no failures that could be traced to flight loading. The only failures found were clearly linked to the harder than expected landing loading. The hard landing resulted in buckling failures within some of the primary structural elements that were subjected to compressive transient compressive forces. The mounting structure for the LOX tank was also found to have sustained substantial damage during landing, with a shear break through one of the three connection elements. This appeared to be consistent with brittle fracture due to the cryogenic temperature it was exposed to, and the shock at landing. There was also some minor damage at the interfaces between the primary structure and composite aeroshell, mostly where bolts secured the stiffer aluminum structure to the composite sections and experienced high transient loading during landing.



Fig. 14 Buckled Aluminum Stringer in Intertank 1

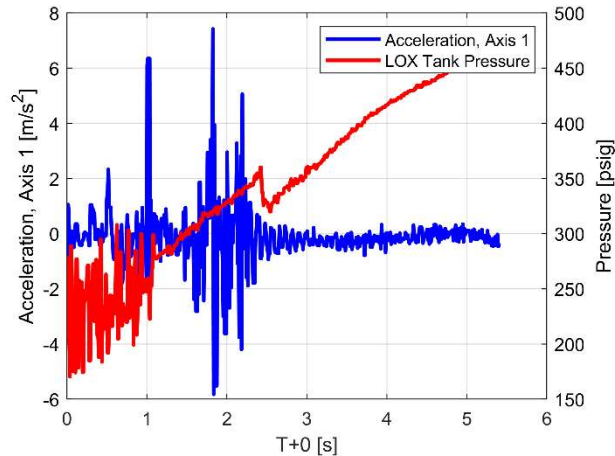


Fig. 15 Lateral Accelerometer and LOX Tank pressure measurements

The onboard accelerometers show substantial structural vibrations caused by the launch rail in the first 2.5 seconds of flight. These vibrations did not appear to have damaged the primary structure but appear to have caused substantial noise in the readings of the COPV pressure and LOX tank pressure on the feed system. For future systems where the tank pressurization is actively controlled, pressure readings are critical to the function of the vehicle propulsion systems. These sensors and their attached pigtail dampers should be mounted more securely to the structure to reduce vibration noise in sensor data.

IX. Conclusion

GoldiLOX’s successful launch and recovery showcases the importance of prioritizing a data rich architecture for a student-built vehicle. Many lessons were learned in the development of GoldiLOX, not only broad programmatic lessons such as testing-like-you-fly or closer cross-team communication, but also individual lessons as students learned the fundamentals of engineering through exciting and challenging experiences. As the Yellow Jacket Space Program looks ahead to their next mission, applying lessons learned from GoldiLOX’s launch is key to creating a more optimized and performance-driven liquid rocket.

Acknowledgments

YJSP would like to thank Dr. Wenting Sun, Dr. Mark Costello, David Wu, and Dr. Glenn Lightsey for their continuous support for YJSP. YJSP also thanks Marotta Controls for their donation of 3 PLV32 solenoid valves used in GoldiLOX. Dozens of students contributed substantially to the design, integration, and launch of GoldiLOX over its three years of development. Former leadership and responsible engineers for this project are listed below.

Amalique Acuna	Shane Dallas	Renee Garg	Mihir Kasmalika	Nikhil Murali	Svanik Tandon
John Henry Adams	Neel Dutta	Joseph Gelin	Samuel Kim	Simon Pahlsmeyer	Frank Wei
Ethan Bravinder	Daniel Elliot	Athreya Gundamraj	Collin Li	Adele Payman	Ben Zabback
Benjamin Breer	Sam Erben	Wyatt Hoppa	Kyle Lundberg	Will Putaansuu	Aaron Hammond
Jurist Chan	Billy Ewles	Celi Johnson	Schuyler McCaa	Jahan Randeria	Sparsh Desai
Trenton Charlson	Philip Fentress	James Jutras	Nicholas McFadden	Noah Robinson	
James Cipolletti	Reid Fly	Cody Kaminsky	Will Miller	Patrick Sliwinski	

References

- [1] Suraj Buddhavarapu, Trenton Charlson, Akhil Gupta and Shrivathsav Seshan. "The Road to the Karman Line: Development of Liquid-Fueled Propulsion and Flight-Control Systems for Suborbital Launch Vehicles," AIAA 2019-0151. *AIAA Scitech 2019 Forum*. January 2019. .
- [2] Abhraneel Dutta, Zach Ernst, Suraj Buddhavarapu, Trenton Charlson, Shrivathsav Seshan and Johnie Sublett. "The Yellow Jacket Space Program: Insights into Starting a Student Led Space-Shot Rocketry Team at the Georgia Institute of Technology," AIAA 2019-0615. *AIAA Scitech 2019 Forum*. January 2019.
- [3] Rutledge, G., Alpert, J., Ebisuzaki, W., "Nomads: A climate and weather model archive at the national oceanic and atmospheric administration," *Bulletin of the American Meteorological Society*, Vol. 87, 2006, pp. 327–341 <https://doi.org/10.1175/BAMS-87-3-327>
- [4] Vallini, L., "Static and Dynamic Analysis of the Aerodynamic Stability and Trajectory Simulation of a Student Sounding Rocket", *Master's Thesis, Universita di Pisa*, 2014.
- [5] Karlgaard, C. D., Kutty, P., and Schoenenberger, M., "Coupled Inertial Navigation and Flush Air Data Sensing Algorithm for Atmosphere Estimation," *Journal of Spacecraft and Rockets*, Vol. 54, No. 1, 2017, pp. 128-140.
- [6] Sutton, George P., *Rocket Propulsion Elements*, 7th ed., Wiley, New York, 2001.
- [7] S. Gordon and B. J. McBride, "Computer Program for Calculation of Complex Chemical Equilibrium Compositions and Applications," NASA,1996.
- [8] J.R. Roebuck, H. Osterberg, "The Joule-Thomson Effect in Nitrogen," *American Physical Society*, Vol. 48, Iss. 5, September 1935.
- [9] Jan-Hendrik Meiss, Jörg Weber, Thierry Kachler, Frank Quinn and Jonathan Paisley. "Electrical Pressurization Concept for the Orion MPCV European Service Module Propulsion System," AIAA 2015-4636. *AIAA SPACE 2015 Conference and Exposition*. August 2015.